Excitons in asymmetric quantum wells

P.S. Grigoryev [a, *], A.S. Kurdyubov [a], M.S. Kuznetsova [a], I.V. Ignatiev [a],
Yu.P. Efimov [b], S.A. Eliseev [b], V.V. Petrov [b], V.A. Lovtcius [b], P.Yu. Shapochkin [b]

[a] *Spin Optics Laboratory, St. Petersburg State University, Ulyanovskaya 1, 198504, St. Petersburg, Russia*
[b] *Department of Physics, St. Petersburg State University, Ulyanovskaya 1, 198504, St. Petersburg, Russia*

ARTICLE INFO

ABSTRACT

Resonance dielectric response of excitons is studied for the high-quality InGaAs/GaAs heterostructures with wide asymmetric quantum wells (QWs). To highlight effects of the QW asymmetry, we have grown and studied several heterostructures with nominally square QWs as well as with triangle-like QWs. Several quantum confined exciton states are experimentally observed as narrow exciton resonances. A standard approach for the phenomenological analysis of the profiles is generalized by introducing different phase shifts for the light waves reflected from the QWs at different exciton resonances. Good agreement of the phenomenological fit to the experimentally observed exciton spectra for high-quality structures allowed us to reliably obtain parameters of the exciton resonances: the exciton transition energies, the radiative broadenings, and the phase shifts. A direct numerical solution of the Schrödinger equation for the heavy-hole excitons in asymmetric QWs is used for microscopic modeling of the exciton resonances. Remarkable agreement with the experiment is achieved when the effect of indium segregation is taken into account. The segregation results in a modification of the potential profile, in particular, in an asymmetry of the nominally square QWs.

© 2016 Elsevier Ltd. All rights reserved.

1. Introduction

Excitons in quantum wells (QWs) have been extensively studied already for four decades [1–7]. Theoretical analysis of the excitons typically assumes a simplified model for the QW potential, e.g., square profiles for electrons and holes [5,8–10]. Real potential, however, is more complex due to several processes taking place during the growth of heterostructures. In the narrow QWs, the monolayer fluctuations of interfaces give rise to fluctuations of the QW width. These fluctuations result in the step-like changes of the exciton quantization energy experimentally observed as a set of exciton resonances in optical spectra [11]. The diffusion of atoms through the QW interface (segregation) during the growth process gives rise to smoothing and an asymmetry of potential profiles for carriers [12,13]. The specially designed asymmetric QWs are also extensively studied in view of their interesting properties, e.g., large electron spin-orbit splitting [14,15], enhanced optical nonlinearity [16–18] and coupling with terahertz radiation [19,20].

The exciton energy and the wave function are sensitive to the potential profile. However, the direct experimental observation of effects of the profile peculiarities on the exciton properties is difficult for several reasons. The exciton energy

---

* Corresponding author.
  E-mail address: f.grigoriev@spbu.ru (P.S. Grigoryev).

shift relative to the theoretically predicted value may be caused, apart from the modification of potential profile, by uncertainties in the QW width and in the composition of the barrier layers within the heterostructure. Various imperfections of the heterostructure like point defects, dislocations, etc., may broaden the exciton resonances and complicate the study of exciton energies. The exciton oscillator strength and the radiative decay rate, which are determined by the exciton wave function, can be studied by reflectance spectroscopy and in the time-resolved experiments [7,21,22]. However, these are the integral characteristics that does not allow one to reconstruct the potential profile when only a single exciton transition is studied.

In this paper, we experimentally study and theoretically analyze reflectance spectra of heterostructures with asymmetric InGaAs/GaAs QWs. We demonstrate that the simultaneous analysis of several exciton resonances in the spectra of relatively wide QWs allows one to obtain valuable information about the potential profile for the excitons. We have developed an approach for the direct numerical solution of the Schrödinger equation for an exciton in a QW with an arbitrary potential profile. The Coulomb electron-hole interaction in the exciton is included into the numerical approach without approximations. Calculations of the exciton energies and wave functions allowed us to accurately model the reflectance spectra using only two fitting parameters describing the maximal indium content in the QW and the characteristic length of the indium diffusion. Both these parameters cannot be controlled and measured during the growth of heterostructures with the high enough accuracy required for the modeling. The obtained agreement allowed us to model the potential profile for excitons and to determine real indium content in the heterostructures under study.

The paper has the following structure. First, we present experimental details and obtained reflectance spectra. A generalization of phenomenological theory of exciton-light coupling for the case of several exciton resonances in a QW with arbitrary potential profile is given in Section 3. Then we compare experimental results and microscopic modeling of the exciton states. Finally, we sum up major results in the Conclusion.

2. Experiment

We have experimentally studied reflectance spectra of several InGaAs/GaAs heterostructures grown by the molecular beam epitaxy (MBE). Two of the structures with the smallest inhomogeneous broadening of exciton resonances have been selected for detailed investigation. The first one (S1) contains a nominally square QW of 95-nm width with small indium content of about 2% grown between the GaAs barrier layers. The second structure, S2, is the specially designed asymmetric InGaAs/GaAs QW with one vertical potential wall and other sloping potential wall. In both structures, effects of the QW asymmetry are found in the comparative study of exciton resonances observed in reflectance spectra. The spectra have been measured using a femtosecond Ti:Sapphire laser or a halogen lamp as a light source. In the latter case, the light was focused onto a 50-μm pin-hole and then refocused onto the sample. The light was directed to the samples at small angle close to the normal incidence. The light spots on the samples were of about 100 μm in both cases. The samples were held in a vacuum chamber of a closed cycle cryostat at $T = 4$ K. The reflected light was dispersed in a 0.55 m spectrometer with the 1800 grooves/mm grating and detected by a nitrogen cooled CCD-matrix. The spectral resolution was of about 30 μeV. To obtain the absolute value of reflectivity, the reflectance coefficient was carefully measured for a single wavelength nearby an exciton resonance using a beam of a continuous wave Ti:sapphire laser focused at the same spot on the sample.
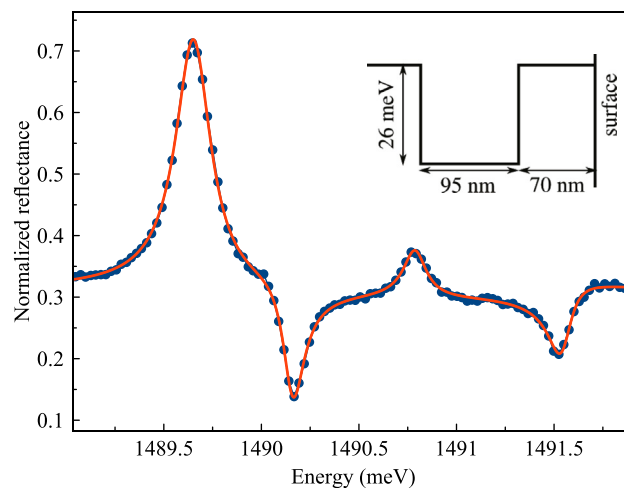

Fig. 1. Reflectance spectrum of InGaAs/GaAs heterostructure with the 95-nm square QW. The red line corresponds to the fit by a phenomenological model with the four free parameters for each resonance. Inset represents the predefined QW potential profile for excitons. (For interpretation of the references to colour in this figure legend, the reader is referred to the web version of this article.)

Fig. 2. Reflectance spectrum of heterostructure with the triangle-like QW (points) and its fit (red line). Inset represents the predefined QW potential profile for excitons. (For interpretation of the references to colour in this figure legend, the reader is referred to the web version of this article.)
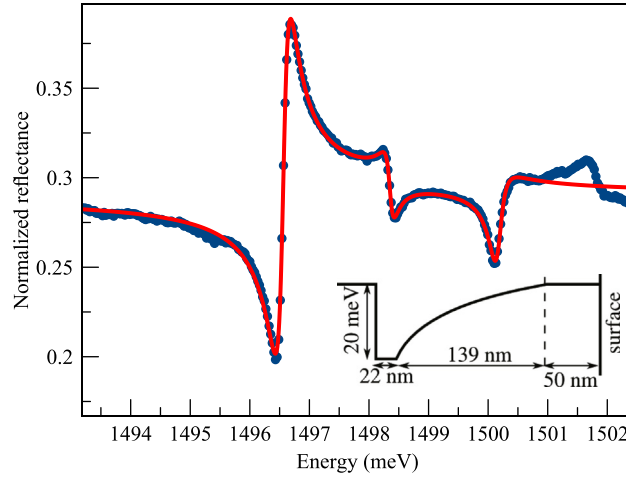
The reflectance spectra for samples S1 and S2 are shown in Figs. 1 and 2, respectively. For sample S1, four exciton reso-nances are clearly seen, two of them as the peaks and two others as the dips. The resonances correspond to optical transitions from the ground state of the system to the quantum confined exciton states in the 95-nm QW. As we discuss in the next section, the different profile of the resonances (peak or dip) is due to the constructive or destructive interference of the light waves reflected from the sample surface and from the QW. The interference strongly depends on the phase shift between the waves, which is different for different exciton transitions. In the spectrum of sample S2, three similar exciton transitions are clearly seen as the resonances. The form of these resonances are more complex and contain valuable information about the phase shifts in this highly asymmetric QW.

The simplified potential profiles for excitons in the QWs are shown in the insets in Figs. 1 and 2. The vertical walls of the QWs were formed during the growth by the rapid opening of the In effusion cell held at a fixed temperature. The sloping potential wall in sample S2 was formed by slow cooling the cell from $T_0 = 754°$ C down to $T_{fin} = 669°$ C with the constant rate, $\gamma_T = 0.0821°$ C/s, so that the In flux was exponentially decreasing. Correspondingly, the indium concentration has been varied according to a phenomenological formula:

$$x_{In}(z) = x_{max}\exp\left[- \left(\gamma_T / \gamma_{gr}\right)z/\delta T_{In}^0\right]. \tag{1}$$

Here $\gamma_{gr} = 0.134$ nm/s is the growth rate of the structure, $\delta T_{In}^0 = 38.54°$ C is a technological parameter of the In cell. A relatively high substrate temperature, $T = 555°$ C used during the growth of the structure results in the noticeable segregation of In, which further complicates the potential profile. The segregation effect will be discussed in Sect. 4

3. Phenomenological analysis

A phenomenological model of resonant reflectance related to a single exciton transition in the symmetric QW is well developed [8,9]. Here we follow the basic theory described in Ref. [5]. The reflectance is governed by the interference of the light waves reflected from the sample surface and the QW layer:

$$R = \left| \frac{r_{01} + r_{QW}e^{i\varphi}}{1 + r_{01}r_{QW}e^{i\varphi}} \right|^2 \tag{2}$$

Here r_{01} and r_{QW} are the amplitude reflectance coefficients from the sample surface and from the QW, respectively. Phase shift φ is determined by the distance from the surface to the QW center:

$$\varphi = 4\pi\left(L_b + L_{QW}/2\right)\sqrt{\varepsilon_b}/\lambda, \tag{3}$$

where L_b is the thickness of the top barrier layer, L_{QW} is the thickness of QW layer, ε_b is the dielectric constant of the layers, and λ is the light wavelength. The r_{01} is considered negative as the sample has larger optical density than the vacuum.

An analytical solution of the Maxwell equation for the light interaction with an exciton in a QW gives rise to the following equation for the amplitude reflectance [5]:

$$r_{QW} = \frac{i\Gamma_0}{\tilde{\omega}_0 - \omega - i(\Gamma + \Gamma_0)} \tag{4}$$

with Γ_0 and $\tilde{\omega}_0$ defined as:

$$\Gamma_0 = \frac{\pi}{2} q\omega_{LT} a_B^3 \left[\int \Phi(z)\cos(qz)\,dz \right]^2, \tag{5}$$

$$\tilde{\omega}_0 = \omega_0 + \frac{\pi}{2} q\omega_{LT} a_B^3 \int \int \Phi(z)\Phi(z')\sin(q|z - z'|)dzdz'. \tag{6}$$

Here ω_0 is the exciton resonance frequency, Γ_0 is the radiative decay rate and Γ is the phenomenologically introduced nonradiative broadening [23]. Function $\Phi(z)$ is the amplitude of exciton wave function when the coordinates of an electron and a hole in the exciton coincide. Quantity q is the wave vector of light, ω_{LT} is the 3D-exciton longitudinal-transverse splitting, and a_B is the exciton Bohr radius.

Eqs. (4–6) are applicable for a single exciton transition in a symmetric QW. They should be generalized for our case of multiple exciton transitions in asymmetric QWs. For the quantum-confined exciton states separated by energy distance, $\Delta E > \Gamma_0 + \Gamma$, a sum over the exciton resonances should be considered [22,24]. Besides, the asymmetry of QW potential gives rise to an additional phase shift ϕ_n for the exciton resonance n. The generalized Eq. (4) acquires the form (see Appendix A for details):

$$r_{QW} = \sum_{n=1}^{n_{max}} \frac{i\Gamma_{0n}e^{i\phi_n}}{\tilde{\omega}_{0n} - \omega - i(\Gamma_n + \Gamma_{0n})}, \tag{7}$$

where

$$\Gamma_{0n} = \frac{\pi}{2} q\omega_{LT} a_B^3 \left(\left[\int \Phi_n(z)\sin(qz)\,dz \right]^2 + \left[\int \Phi_n(z)\cos(qz)\,dz \right]^2 \right). \tag{8}$$

As seen, two exciton-light overlapping integrals appear in the expression for Γ_{0n} in the case of asymmetric potential [comp. with Eq. (5)]. When the QW potential is symmetric, only one integral containing $\cos(qz)$ for exciton states $n = 1,3,\ldots$ or $\sin(qz)$ for exciton states $n = 2,4,\ldots$ is non-zero.

Phase shift ϕ_n is determined by ratio of the integrals:

$$\tan\frac{\phi_n}{2} = \frac{\displaystyle\int \Phi_n(z)\sin(qz)\,dz}{\displaystyle\int \Phi_n(z)\cos(qz)\,dz}. \tag{9}$$

As seen this expression also includes both $\cos(qz)$ and $\sin(qz)$. Phases ϕ_n can be used as a measure of the asymmetry of the potential profile. In the symmetric QW, they all should be zero for exciton states $n = 1,3,\ldots$ and π for states $n = 2,4,\ldots$ However in the experiment, they can be determined up to a constant phase shift φ defined by Eq. (3). We, therefore, consider phases

$$\tilde{\phi}_n = \phi_n + \varphi, \tag{10}$$

which are directly determined from the experimental spectra fitting them by Eqs. (2) and (7).

We have fitted several exciton resonances observed in the reflectance spectra of the heterostructures studied. Results are shown in Figs. 1 and 2. Respective fitting parameters are listed in Tables 1 and 2 As seen from the figures, the fit by Eqs. (2) and (7) allows us to accurately reproduce the spectra for both samples in the spectral range of several excitonic resonances. We did not fit the fourth exciton resonance for the triangle QW (see the spectral peculiarity in the range 1501−1502 meV in Fig. 2) because it is superimposed on the 2s-exciton transition not analyzed in present work. The obtained results support the generalization of the phenomenological model suggested. We also may conclude that the parameters obtained in the fitting are reliably determined.

As seen from Table 1 for the square QW, phases $\tilde{\phi}_n$ for states $n = 1,3$ are close to each other and small while for states $n = 2,4$ they are close to π. This indicates that the asymmetry of this QW in not large. In the case of the triangular QW (see Table 2), the phase difference is much larger that clearly shows sensitivity of the phases to the QW asymmetry. The quantitative analysis of the phases will be done in the next section after the microscopic modeling of the exciton states is described.

Table 1

Fitting parameters extracted from the experiment for the square QW versus those obtained in the microscopic modeling. Parameters of the modeling: $L_b = 70$ nm, $L_{QW} = 95$ nm, $x_{max} = 1.89\%$, $\lambda = 3.75$ nm. The common phase shift 2π is subtracted from phases $\bar{\phi}_n$.

		X1	X2	X3	X4
$\hbar\bar{\omega}_{0n}$ (meV)	Exp.	1489.65	1490.16	1490.79	1491.55
	Comp.	1489.69	1490.15	1490.80	1491.61
$\hbar\Gamma_{0n}$ (μeV)	Exp.	47.2	19.1	6.9	11.1
	Comp.	50.8	18.8	4.3	8.2
$\hbar\Gamma_n$ (μeV)	Exp.	37.7	59	61	67
$\bar{\phi}_n$ (rad)	Exp.	0.16	3.10	0.14	3.70
	Comp.	0.16	3.29	0.23	3.29

4. Microscopic modeling

We consider the problem of an exciton in a QW described by the stationary Schrödinger equation for two particles (electron and hole) with Coulomb interaction. The wave function of the exciton can be expressed in planar heterostructures as:

$$\psi(X, Y, z_e, z_h, \rho, \varphi) = e^{iK_X X + iK_Y Y} \psi(z_e, z_h, \rho) e^{ik_\varphi \varphi} \tag{11}$$

with X and Y as the center-of-mass coordinates in the XY plane, z_e and z_h as the electron and hole coordinates in the growth direction, respectively. Quantities ρ and φ are the polar coordinates of relative electron-hole motion in the plane perpendicular to the growth axis. Quantity k_φ is the z-projection of the exciton angular momentum. We suggest it to be zero for the optically observable exciton states (s-like states).

Function $\psi(z_e, z_h, \rho)$ is the eigenfunction of operator:

$$\widehat{H} = \widehat{K} + V_e f(z_e) + V_h f(z_h) - \frac{e^2}{\varepsilon \sqrt{\rho^2 + (z_e - z_h)^2}}. \tag{12}$$

Here $\varepsilon = 12.56$ is the dielectric constant for GaAs, $f(z)$ is the QW potential function, V_h and V_e are the valence and conduction band offsets, respectively, at the point where $f(z) = 1$. We assume that $V_e = 2V_h$ for all the In concentrations considered. To calculate the potential well for excitons, we use a phenomenological dependence of the band gap for solid solution In$_x$Ga$_{1-x}$As on the indium concentration x [25]:

$$E_g(x) = E_g(\text{InAs})x + E_g(\text{GaAs})(1 - x) - 0.477x(1 - x) + (a_c - a_v)\sum_i \varepsilon_{ii} - b\left(\varepsilon_\| - \varepsilon_{zz}\right), \tag{13}$$

where $E_g(\text{GaAs}) = 1.519$ eV and $E_g(\text{InAs}) = 0.417$ eV are the band gaps for GaAs and InAs, respectively. The last two terms in Eq. (13) represent the strain-induced variation of the band gap, where a_c, a_v and b are the deformation potentials for the In$_x$Ga$_{1-x}$As crystal obtained by the linear interpolation of parameters from Table 3. Components of the deformation tensor ε depend on the indium content in the InGaAs QW. Simple formulas for the case of the single InGaAs QW grown at the [001] substrate follow from Ref. [26]:

$$\varepsilon_\| = \varepsilon_{xx} = \varepsilon_{yy} = \frac{a(x)}{a_{\text{GaAs}}} - 1,$$
$$\varepsilon_{zz} = 1 - 2\frac{c_{12}(x)}{c_{11}(x)}\varepsilon_{xx}, \tag{14}$$

where $a(x)$ and a_{GaAs} are the lattice constants of the unstrained In$_x$Ga$_{1-x}$As and GaAs, respectively, $c_{11}(x)$ and $c_{12}(x)$ are the In$_x$Ga$_{1-x}$As elastic constants. Each of six parameters from Table 3 is included in Eqs. (13 and 14) as a linear interpolation on the indium content, therefore $E_g(x)$ acquires rather complex dependence on x. It is even further complicated due to the piezo-electric effect in a general case [27]. However for the structures grown on the [001] substrate, no piezo-induced electric field appears in the structure.

The bottom of potential well for excitons is determined as

$$V(x) \equiv V_e + V_h = E_g(\text{GaAs}) - E_g(x). \tag{15}$$

The profile of QW potential is determined by function $f(z)$, which will be discussed below.

Operator $\widehat{K}$ in Eq. (12) consists of three terms:

Table 2

Fitting parameters extracted from the experiment for the triangular QW versus those obtained in microscopic modeling. In the microscopic modeling we used: $L_b = 50$ nm, $L_1 = 22$ nm, $L_2 = 139$ nm, $x_{max} = 1.49\%$, $\lambda = 4.5$ nm. The common phase shift 2π is subtracted from phases $\bar{\phi}_n$.

		X1	X2	X3
$\hbar\tilde{\omega}_{0n}$ (meV)	Exp.	1496.581	1498.355	1500.170
	Comp.	1496.61	1498.16	1499.55
$\hbar\Gamma_{0n}$ (μeV)	Exp.	31.5	4.0	8.1
	Comp.	36.3	7.1	9.8
$\hbar\Gamma_n$ (μeV)	Exp.	99	84	124
$\bar{\phi}_n$ (rad)	Exp.	4.61	8.15	3.84
	Comp.	4.61	8.2	3.78

$$\widehat{K} = -\frac{\hbar^2}{2m_e}\frac{\partial^2}{\partial z_e^2} - \frac{\hbar^2}{2m_{z_h}}\frac{\partial^2}{\partial z_h^2} - \frac{\hbar^2}{2\mu_{xy}}\Delta_\rho. \tag{16}$$

Here Δ_ρ is the Laplacian in polar coordinates for the case $k_\varphi = 0$:

$$\Delta_\rho = \frac{1}{\rho}\frac{\partial}{\partial\rho}\left(\rho\frac{\partial}{\partial\rho}\right) \tag{17}$$

In the GaAs-based heterostructures, the conduction band can be considered as an isotropic one with an effective electron mass $m_e = 0.0665\,m_0$. The valence band is twice degenerate, consists of heavy-hole and light-hole subbands, and is described in terms of the Luttinger Hamiltonian [28]. The effect of quantum confinement breaks the valence band degeneracy, which results in the anisotropic heavy-hole and light-hole masses. The InGaAs/GaAs QWs are also affected by a strain due to the mismatch of lattice constants of InAs and GaAs crystals, which induces the heavy-hole-light-hole splitting up to 10 meV for the 2% In concentration in the QWs [26]. This splitting effectively reduces the heavy-hole-light-hole interaction, therefore we can introduce the heavy hole masses in growth direction and in xy-plane, respectively: $m_{z_h} = m_0/(\gamma_1 - 2\gamma_2)$ and $m_{xy_h} = m_0/(\gamma_1 + \gamma_2)$. The reduced exciton mass in xy-plane $\mu_{xy} = m_{xy_h}m_e/(m_{xy_h} + m_e)$. Due to the low indium concentration, we use the GaAs Luttinger parameters suggested by Vurgaftman et al. [25]: $\gamma_1 = 6.95$, $\gamma_2 = 2.06$.

The QW potential profile defined by $f(z)$ function is known to be significantly modified by the segregation effect in the InGaAs/GaAs QWs [13,29–31]. The indium atoms are more mobile during the growth process as compared to the gallium atoms. This results in a diffusion of the indium atoms from lower layers of growing structure to the higher ones. Related modification of the QW potential can be well described using only a single parameter, λ_D [13]. This parameter is the indium diffusion length, which characterizes the exponentially decaying indium concentration after deposition of the δ-layer of In: $x(z) = x(0)\exp(-z/\lambda_D)$. It depends on the growth conditions, in particular, on the substrate temperature and varies in the range $\lambda_D = 1.5\ldots4.5$ nm for temperatures $T = 500\ldots550^\circ$ C. We use this parameter as the free one in the modeling of exciton spectra.

In the framework of the phenomenological model, the segregation process can be described by a simple rate equation for In concentration, $x(z)$, as a function of coordinate z along the growth direction:

$$\frac{dx(z)}{dz} = -\frac{x(z)}{\lambda_D} + \frac{F_{In}(z)}{\lambda_D}. \tag{18}$$

Here $F_{In}(z)$ is the In flux with taking into account the sticking coefficient. The flux is varied during the growth process in a general case.

The general solution of Eq. (18) is:

$$x(z) = e^{-z/\lambda_D}\int_{z0}^{z} e^{z'/\lambda_D}\frac{F_{In}(z')}{\lambda_D}\,dz'. \tag{19}$$

Here z_0 is the coordinate where the indium containing layers start to grow.

In the particular case of square QW, the indium flux $F_{In}(z) = F_{In}^0$ within the QW and zero outside it. The integration in Eq. (19) gives rise to a solution:

$$x(z) = F_{In}^0\left(1 - e^{-z/\lambda_D}\right), \quad 0 < z < L_{QW},$$
$$x(z) = F_{In}^0\left(1 - e^{-L_{QW}/\lambda_D}\right)e^{-(z-L_{QW})/\lambda_D}, \quad z > L_{QW}. \tag{20}$$

Here L_{QW} is the nominal QW width. This solution coincides with that presented in Ref. [13].

Table 3
Deformation potentials, lattice constants and elastic constants used in the calculations, see Ref. [25].

	a_c (eV)	a_v (eV)	b (eV)	a (nm)	c_{11} (GPa)	c_{12} (GPa)
GaAs	−7.17	−1.16	−2	0.564	1221	566
InAs	−5.08	−1.0	−1.8	0.605	832.9	452.6

The potential function $f(z)$ [see Eq. (12)] is expressed via x(z):

$$f(z) = 1 - \frac{x(z)}{x_{max}}, \tag{21}$$

where x_{max} is the In concentration in the bottom of potential well. The potential profile for excitons in square QW under study modeled by this way is shown in Fig. 3. We have manually shifted this profile down by the bulk exciton binding energy, $E_x = 4.2$ meV, to clearly demonstrate the quantum confined effect for excitons.

Using function $f(z)$, we find several lowest eigenstates of the eigenproblem with operator (12). We represent this operator as a matrix composed according to the 3-point finite difference representation of differential operators. Computation area is $200 \times 200 \times 400$ nm^3 with $70 \times 70 \times 200$ points along the z_e, z_h, and ρ coordinates, respectively. The Arnoldi algorithm realization in the ARPACK library was used to obtain the eigenstates. Further technical details of the numerical calculations can be found in Refs. [7,32].

For the square QW potential smoothed by the segregation, we varied the depth of the QW potential, $V = V_e + V_h$, see Eq. (12), and the In diffusion length λ_D to obtain the best correspondence of calculated energies of the quantum confined states with those found experimentally. We should note that the variation of parameter V mainly gives rise to the overall energy shift of exciton levels with small change of energy gaps between them. This is due to the relatively deep potential well, $V \approx 26$ meV, relative to the energy range in a few meV for exciton states under study, see Fig. 3. The calculated exciton energies, $\hbar\omega_n$, should be corrected due to exciton-light coupling using Eq. (6). We found, however, that this correction is negligibly small, a few tens of μeV, and can be omitted.

The energy difference between the neighboring exciton levels, $\Delta E_{nn'} = \hbar\tilde{\omega}_{n'} - \hbar\tilde{\omega}_n$, in particular, the difference ΔE_{12}, is very sensitive to parameter λ_D, because of sensitivity of curvature of the potential near the bottom, see Fig. 3. When one neglects the segregation, this energy difference is noticeably smaller than the difference obtained from the experiment. These properties of exciton spectrum allow one to obtain parameters V and λ_D independently.

The calculated energies are shown in Fig. 3 and also present in Table 1. As seen, the calculated and measured energies coincide with the accuracy in several tens of μeV. We would like to stress that this correspondence has been achieved by the variation of only two fitting parameters.

The figure also shows functions $\Phi_n(z)$ obtained in the numerical computations. They are shifted vertically according to the calculated energies. We should note one more effect of segregation, namely, the stronger penetration of functions $\Phi_n(z)$ to the left barrier compared to the right one.
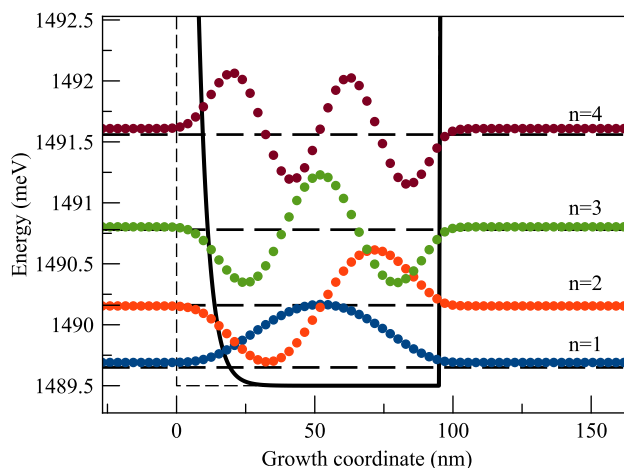

Fig. 3. Segregated QW potential (black solid line) and functions $\Phi(z)$ (colored dots) for the first four excitonic states. The thin dashed line shows an initial profile of the square QW. The dashed horizontal lines correspond to the exciton energies extracted from the reflectance spectrum shown in Fig. 1. (For interpretation of the references to colour in this figure legend, the reader is referred to the web version of this article.)

The obtained functions $\Phi_n(z)$ allowed us to calculate radiative broadenings, $\hbar\Gamma_{0n}$, using Eq. (8). They are compared with the experimentally obtained data in Table 1. As seen the calculated radiative broadenings are in good agreement with the experimental data.

Phases ϕ_n have been calculated by the use of Eq. (9). A constant phase φ has been added to phases ϕ_n to take into account the phase shift during propagation of light wave from the sample surface to the QW and back. This constant phase is defined by the Eq. (3). However, due to possible layer width variation, we have used phase φ as a fitting parameter to set phase $\tilde{\phi}_1$ equal to the experimentally obtained value. Experimentally obtained φ differs from that predicted by Eq. (3) by 2%. The calculated phases are close to those obtained from the experiment for all four resonances in this structure. There is some discrepancy with the phase for the fourth resonance obtained from the experiment. The possible reason for that is a complexity of experimental spectrum in the vicinity of this resonance, which can be superimposed on the transition to the 2s exciton state originated from the lowest quantum confined exciton state.

The calculated parameters $\hbar\Gamma_{0n}$ and ϕ_n have been used to simulate, exploiting Eq. (2), the reflectance spectrum for structure with the square QW. The only parameters additionally taken are: the nonradiative broadening $\hbar\Gamma_n = 40\ \mu eV$ for all the resonances (compare with Table 1), the effective top barrier layer L_b=70 nm defining phase φ [see Eq. (3)], and the dielectric constant ε_b=12.56 defining the reflectance beyond the exciton resonances. Results of the theoretical modeling are compared with the experiment in Fig. 4. As seen, the modeling accurately reproduces all the features of the experimental spectrum.

Similar microscopic modeling has been done for sample S2 with the triangle-like QW. The segregated potential profile in this case can be easily calculated using general solution (19). The obtained profile is shown in Fig. 5. This figure also demonstrates calculated energies as well as functions $\Phi_n(z)$ for the quantum-confined excitonic states. The discrepancy of the calculated energies with the measured ones is also negligibly small (see Table 2) that indicates that the potential profile of the QW is correctly modeled. The microscopic modeling also allowed us to calculate the radiative broadenings and phase shifts for the exciton transitions. Value φ in calculated phase is tuned to make phase $\tilde{\phi}_1$ equal to the experimentally obtained value. Difference in experimentally defined φ from that predicted by Eq. (3) in this case is of about 7%. They are compared with the experiment in Table 2. As seen, good agreement is observed for the data.

Using the calculated quantities, we have simulated the reflectance spectrum for this sample. It is shown in Fig. 6. Good correspondence of the calculated and experimental spectra is observed that supports the proposed model of potential profile.

5. Conclusion

Our study of exciton resonances in the reflectance spectra of heterostructures with the InGaAs QWs shows that the careful comparison of experimental data with results of the microscopic modeling allows one to determine the potential profile for excitons with high accuracy. We have experimentally studied and theoretically modeled several exciton resonances in reflectance spectra of two samples with asymmetric InGaAs/GaAs QWs. The analysis shows that even in the nominally symmetric square QW (sample S1), the segregation of indium during the MBE growth of the structure results in an asymmetry of the QW potential profile. This asymmetry reveals itself in a change of energy gaps between the neighboring quantum-confined excitonic levels. At the same time, no valuable change of phase shifts for different exciton transitions is observed for this sample.
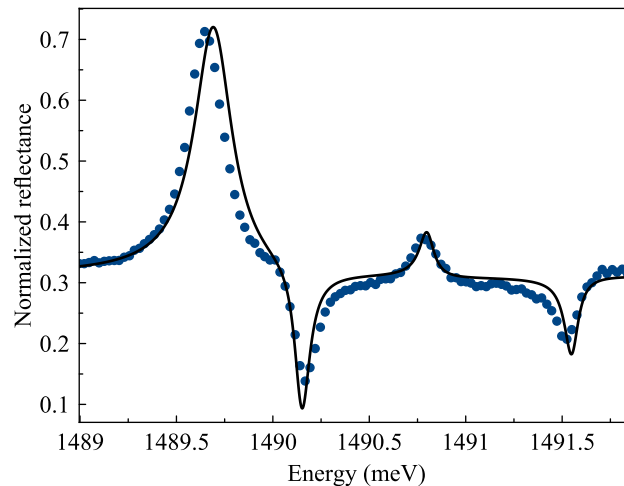

Fig. 4. The comparison of theoretically modeled reflectance spectrum of InGaAs/GaAs heterostructure with the square QW (solid line) and that measured experimentally (line with points). The theoretical spectrum is calculated using Eq. (2) and parameters for exciton resonances obtained in microscopic calculation (see Table 1). Parameters of non-radiative broadening, $\hbar\Gamma_\mathbf{n}$, have been taken 40 μeV for all the resonances.
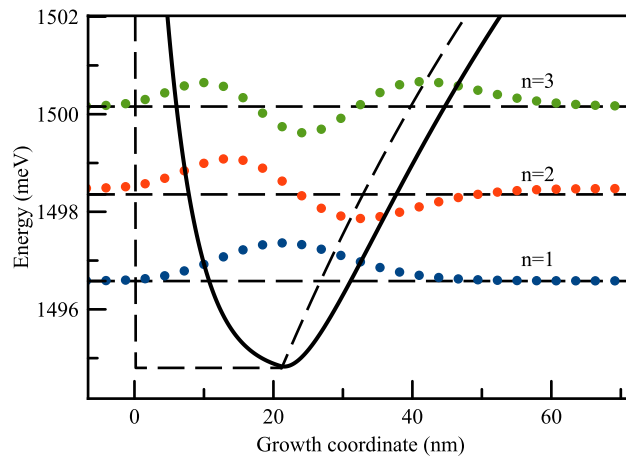
Fig. 5. Segregated asymmetric QW potential and $\Phi(z)$ wave functions of first three states. Dashed horizontal lines correspond to energies extracted from spectrum in Fig. 2.
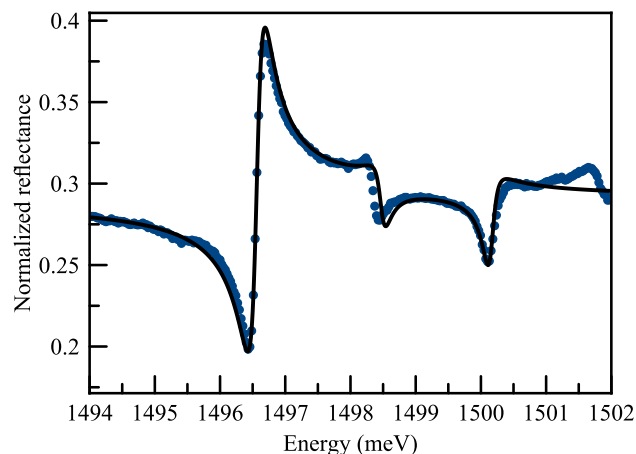

Fig. 6. Reflectance spectrum of heterostructure with the asymmetric QW. Black line is the spectrum obtained using Eq. (2). Parameters for each exciton resonance were obtained in microscopic calculation (see Table 2). As $\hbar\Gamma_n$ parameter we used 100 μeV for all resonances.

For the sample with the triangle-like QW, both the energy position of the exciton resonances and their phases are very sensitive to the potential profile. This sensitivity allows one to reliably model the potential profile exploiting only a few free parameters. The important parameters are the indium content in the bottom of QWs, x_{max}, and the segregation diffusion length, λ_D. The analysis performed shows that the exciton resonances are highly sensitive to these parameters so that the accuracy of their determination using the method described in present work significantly exceeds accuracy of other methods.

The simulated reflectance spectra are in the good agreement with the experimentally observed ones. This means that all the valuable processes are included in the modeling. In fact, the key process in the structures studied is the exciton-light coupling determining the radiative broadening of exciton resonances, $\hbar\Gamma_{0n}$, and the phase shifts, ϕ_n, of light wave during the reflection from the QW. The nonradiative broadening, $\hbar\Gamma_n$, cannot be modeled in the framework of the proposed approach. However, the relatively small difference of their values for different exciton states and a slow monotonic rise with number of exciton state indicates that most probable origin of the broadening is the exciton-phonon scattering. Further studies are needed to model this process.

Finally we should stress that the study of several exciton resonances allows one to reliably determine the potential profile of the QW localizing the excitons. Both the exciton energies and the light phases contain valuable information about the profile.

Acknowledgments

Appendix A. Exciton-induced resonant reflectance

The amplitude reflection coefficient for a QW, r_{QW}, arises from the solution of wave equation for electric field of light, E, in heterostructure:

$$\frac{d^2E}{dz^2} = -\left(\frac{\omega}{c}\right)^2 [\varepsilon_b E + 4\pi P_{exc}(z)], \tag{A.1}$$

where $P_{exc}(z)$ is a nonlocal dielectric polarization of exciton given by equations [5]:

$$4\pi P_{exc}(z) = G(\omega)\Phi(z) \int \Phi^*(z')E(z')dz', \tag{A.2}$$

$$G(\omega) = \frac{\pi \varepsilon_b \omega_{LT} a_B^3}{\hbar(\omega_0 - \omega - i\Gamma)}$$

Function $\Phi(z)=\Phi^*(z)$ is defined as

$$\Phi(z) = \varphi(z, z, 0), \tag{A.3}$$

where $\varphi(z_e, z_h, \rho)$ is the exciton wave function, which satisfy a Schrödinger equation with Hamiltonian (12).

The solution of Eq. (A.1) with function $P_{exc}(z)$ is given by formula [5]:

$$E(z) = E_0 e^{iqz} + i\frac{q_0^2}{2q} G(\omega)\Lambda \int e^{iq|z-z'|}\Phi(z')dz', \tag{A.4}$$

where $q_0=\omega/c$ and $q = (\omega/c)\sqrt{\varepsilon_b}$ are the light wave vectors in vacuum and in the QW, respectively. The first term in this equation describes the light wave with amplitude of electric field E_0 incident on the QW from the left side. The second term is the secondary wave induced by the exciton in the QW. Quantity Λ is:

$$\Lambda = \frac{E_0 \int \Phi(z) e^{iqz} dz}{1 - iq_0^2/(2q)G(\omega) \int\int e^{iq|z-z'|}\Phi(z)\Phi(z')dzdz'}. \tag{A.5}$$

In contrast to Ref. [5] we do not assume any parity of function $\Phi(z)$ and, therefore, keep function $\exp(iqz)$ in the numerator of this expression rather than it even part, $\cos(qz)$, compare with Eq. (3.17) in Ref. [5]. Using definitions for $\tilde{\omega}_0$, Eq. (6), and Γ_0, Eq. (8), we obtain:

$$\Lambda = E_0 \frac{(\omega_0 - \omega - i\Gamma) \int \Phi(z) e^{iqz} dz}{\tilde{\omega}_0 - \omega - i(\Gamma + \Gamma_0)}. \tag{A.6}$$

The coefficient of amplitude reflectance from the QW is the ratio of the second and first terms in Eq. (A.4):

$$r_{QW} = \frac{i\frac{\pi}{2} q \omega_{LT} a_B^3 \left[\int \Phi(z) e^{iqz} dz \right]^2}{\tilde{\omega}_0 - \omega - i(\Gamma + \Gamma_0)}, \tag{A.7}$$

The numerator of this equation can be expressed as $i\Gamma_0\exp(i\phi)$, where ϕ is defined by Eq. (9). For symmetric QWs, function $\Phi(z)$ is even or odd depending on the number n of the quantum-confined state. Correspondingly, phase $\phi=0$ or π. Summing contributions (A.7) to the reflection from several exciton resonances, we obtain final expression (7).

References

[1] R. Dingle, W. Wiegmann, C.H. Henry, Quantum states of confined carriers in very thin $Al_xGa_{1-x}As$–$GaAs$–$Al_xGa_{1-x}As$ heterostructures, Phys. Rev. Lett. 33 (1974) 827.
[2] S.B. White, L.J. Sham, Electronic properties of flat-band semiconductor heterostructures, Phys. Rev. Lett. 47 (1981) 879.
[3] G. Bastard, Wave Mechanics Applied to Semiconductor Heterostructures, Les Editions de Physique, 1988, p. 356 pp. Published by.
[4] J.H. Davies, The Physics of Low-dimensional Semiconductors. An Introduction, Cambridge university press, 1998, p. 438 pp.
[5] E.L. Ivchenko, Optical Spectroscopy of Semiconductor Nanostructures, Springer, Berlin, 2004, p. 437 p.

[6] A.V. Kavokin, J.J. Baumberg, G. Malpuech, F.P. Laussy, Microcavities, Oxford university press, 2011, p. 467 pp.
[7] E.S. Khramtsov, P.S. Grigoryev, I.V. Ignatiev, S. Yu Verbin, P.A. Belov, S.A. Eliseev, Yu P. Efimov, V.A. Lovtcius, V.V. Petrov, S.L. Yakovlev, Radiative decay rate of excitons in square quantum wells: microscopic modeling and experiment, J. Appl. Phys. 119 (2016) 184301.
[8] L.C. Andreani, F. Tassone, F. Bassani, Radiative lifetime of free excitons in quantum wells, Solid State Commun. 77 (1991) 641.
[9] Fiz. Tverd. Tela 33, 2388 E.L. Ivchenko, Excitonic polaritons in periodic quantum-well structures, Sov. Phys. Solid State 33 (1991) 1344.
[10] F. Tassone, F. Bassani, L.C. Andreani, Quantum-well reflectivity and exciton-polariton dispersion, Phys. Rev. B 45 (1992) 6023.
[11] D. Gammon, E.S. Snow, B.V. Shanabrook, D.S. Katzer, D. Park, Homogeneous linewidths in the optical spectrum of a single gallium arsenide quantum dot, Science 273 (1996) 8790.
[12] J.M. Moison, C. Guille, F. Houzay, F. Barthe, M. Van Rompay, Surface segregation of third-column atoms in group III-V arsenide compounds: ternary alloys and heterostructures, Phys. Rev. B 40 (1989) 6149.
[13] K. Muraki, S. Fukatsu, Y. Shiraki, R. Ito, Surface segregation of in atoms during molecular beam epitaxy and its influence on the energy levels in InGaAs/GaAs quantum wells, Appl. Phys. Lett. 61 (1992) 557.
[14] E.A. de Andrada e Silva, G.C. La Rocca, F. Bassani, Spin-orbit splitting of electronic states in semiconductor asymmetric quantum wells, Phys. Rev. B 55 (1997) 16293.
[15] Dirk Grundler, Large rashba splitting in InAs quantum wells due to electron wave function penetration into the barrier layers, Phys. Rev. Lett. 84 (2000) 6074.
[16] E. Rosencher, Ph Bois, Model system for optical nonlinearities: asymmetric quantum wells, Phys. Rev. B 44 (1991) 11315.
[17] R. Atanasov, F. Bassani, V.M. Agranovich, Second-order nonlinear optical susceptibility of asymmetric quantum wells, Phys. Rev. B 50 (1994) 7809.
[18] Hui Sun, Shuangli Fan, Hongjun Zhang, Shangqing Gong, Tunneling-induced high-efficiency four-wave mixing in asymmetric quantum wells, Phys. Rev. B 87 (2013) 235310.
[19] M. Bedoya, A.S. Camacho, Nonlinear intersubband terahertz absorption in asymmetric quantum well structures, Phys. Rev. B 72 (2005) 155318.
[20] Simone De Liberato, Cristiano Ciuti, Chris C. Phillips, Terahertz lasing from intersubband polariton-polariton scattering in asymmetric quantum wells, Phys. Rev. B 87 (2013) 241304(R).
[21] S.V. Poltavtsev, Yu P. Efimov, Yu K. Dolgikh, S.A. Eliseev, V.V. Petrov, V.V. Ovsyankin, Extremely low inhomogeneous broadening of exciton lines in shallow (In,Ga)As/GaAs quantum wells, Solid State Commun. 199 (2014) 47.
[22] A.V. Trifonov, S.N. Korotan, A.S. Kurdyubov, I. Ya Gerlovin, I.V. Ignatiev, Yu P. Efimov, S.A. Eliseev, V.V. Petrov, Yu K. Dolgikh, V.V. Ovsyankin, A.V. Kavokin, Nontrivial relaxation dynamics of excitons in high-quality InGaAs/GaAs quantum wells, Phys. Rev. B 91 (2015) 115307.
[23] Only the homogeneous nonradiative broadening may be taken into account by this way. This broadening may be caused, in particular, by the phonon-mediated ejection of excitons beyond the light cone [22]. Besides, inhomogeneous broadening may take place. Its consideration requires a convolution of $r_{QW}(\omega)$ with a distribution function describing the exciton statistics in the inhomogeneous ensemble. In our paper, we study the high-quality samples, in which the inhomogeneous broadening is smaller than $\Gamma+\Gamma_0$.
[24] Here we have omitted factor $(-1)^{n-1}$, which is present in similar equation in Ref. [22]. For the strongly asymmetric QWs considered in present paper, classification of exciton states by their parity is not applicable any more.
[25] I. Vurgaftman, J.R. Meyer, L.R. Ram-Mohan, Band parameters for III–V compound semiconductors and their alloys, J. Appl. Phys. 89 (2001) 5185.
[26] Chris G. Van de Walle, Band lineups and deformation potentials in the model-solid theory, Phys. Rev. B 39 (1989) 1871.
[27] P. Bigenwald, B. Gil, Excitonic properties and resonance widths in biased (Ga,In)As-GaAs double quantum wells, Phys. Rev. B 51 (1995) 9780.
[28] J.M. Luttinger, Quantum theory of Cyclotron resonance in semiconductors: general theory, Phys. Rev. 102 (1956) 1030.
[29] S. Martini, A.A. Quivy, E.C.F. da Silva, J.R. Leite, Real-time determination of the segregation strength of indium atoms in InGaAs layers grown by molecular-beam epitaxy, Appl. Phys. Lett. 81 (2002) 2863.
[30] Yu N. Drozdov, N.V. Baǐdus, B.N. Zvonkov, M.N. Drozdov, O.I. Khrykin, V.I. Shashkin, Segregation of Indium in InGaAs/GaAs Quantum Wells Grown by Vapor-Phase Epitaxy, Fiz. Tekhn. Polupr. 37, 203, Semiconductors 37 (No. 2) (2003) 194199.
[31] S. Martini, J.E. Manzoli, A.A. Quivy, Study of the influence of indium segregation on the optical properties of InGaAs/GaAs quantum wells via split-operator method, J. Vac. Sci. Technol. B 28 (2010) 277.
[32] E.S. Khramtsov, P.A. Belov, P.S. Grigoryev, I.V. Ignatiev, S. Yu. Verbin, S.L. Yakovlev, Theoretical modeling of exciton-light coupling in quantum wells, J. Phys. Conf. Ser. 690 (2016) 012018.